COBEM 2023 27TH INTERNATIONAL CONGRESS OF MECHANICAL ENGENEERING

ABCM Brazilian Society of Mechanical Sciences and Engineering
27th ABCM International Congress of Mechanical Engineering
December 04-08, 2023, Florianópolis-SC, Brazil

COB-2023-1801
WALL TEMPERATURE INFLUENCE ON CONFINED LAMINAR EQUIDIFFUSIONAL JET FLAMES

Ricardo L. Soares-Júnior
Albino J. K. Leiroz
Department of Mechanical Engineering – POLI/ COPPE
Federal Universit of Rio de Janeiro – UFRJ
PO Box 68503, Rio de Janeiro, Rio de Janeiro, 21941-972, Brazil
riclsoaresjr@mecanica.coppe.ufrj.br, leiroz@mecanica.coppe.ufrj.br

Abstract. *The present work evaluates the effects of burner surrounding wall temperature on an axisymmetric confined laminar reactive flow characteristics using an extension of the classic Shvab-Zel'dovich formulation. The limiting case of the unity Lewis numbers and adiabatic wall is considered to isolate the surrounding wall temperature effects in the reactive flow. Besides, a global, single-step, irreversible and infinitely fast reaction of methane-in-air combustion is considered. The Finite Volume Method is employed to solve the governing equations in a structured mesh., with WUDS (Weighted Upstream Differencing Scheme) being applied for the discretization of convective terms and the SIMPLEC (Semi-Implicit Method for Pressure Linked Equations-Consistent) method for treating the pressure-velocity coupling, Results are obtained for a Reynolds number of 371.6 and surrounding wall temperatures ranging from 373 K to 1523 K, allowing for analysis of changes on flow structures and on flame height and width. Additionally, results also show the axial evolution of the mean flow temperature and of the Nusselt number along the surrounding contour for the observed over-ventilated flames. A non-monotonic behavior of the axial mean flow temperature profiles is observed due to heat release from the combustion chemical reaction. Furthermore, due to the combined effects of the wall heat flux and of the axial mean flow temperature axial distribution, discontinuities in the Nusselt number profiles along the surrounding solid contour are also observed from the obtained results.*

Keywords: *Wall Temperature Effects, Diffusion Flame, Flame Sheet Model, Finite Volume Method*

1. INTRODUCTION

Non-premixed laminar jet flames are present in a wide variety of equipments and industrial applications usually associated with turbulent flows (Williams, 1985). Although a deep understanding of the combustion process is critical for an effective reduction of pollutant emissions and for enhancements in equipment thermal efficiency, the numerical solutions for detailed mathematical models of this phenomenon still represent a challenge of elevated computational cost. The study of simpler laminar jet diffusion flames may provide relevant information about the physical and chemical process involved in several systems of interest (Smooke, 2013; Zadsirjan et al., 2020).

Burke and Schumann (1928) introduced the classical laminar diffusion flame model for rectangular and cylindrical burner geometries. The Burke-Schumann model, which allowed analytical solutions, was extended to consider the energy transport and exhaustively applied in cylindrical laminar flames (Chung and Law, 1984), and providing reasonable predictions for flame shape and height (Kuo, 2005).

The work presented by Mitchell et al. (1980) for a reactive laminar concentric confined jets showed a comparison between numerical and experimental results. The flame sheet model was employed. Besides, thermophysical variation properties and multidimensional diffusive and convective effects were considered. The vorticity-stream formulation was used for the flow field description. The Finite Difference Method (FDM) and Alternating Direction Implicit (ADI) were applied for the numerical solution for the resulting algebraic system of equations. The numerical results showed good agreement with the numerical data. Besides, the mathematical model was capable to capture the effects of both reactants flow rate and burner diameter variation, and of reactants preheating.

A primitive variable approach was use by Xu and Smooke (1993) to describe the flow field of a laminar diffusion jet flame problem. The reactive flow was numerically resolved using the Newton Method and the SIMPLER interactive scheme (Patankar, 1980). The results were initially obtained considering the flame sheet model and variations of thermophysical property described by simple analytical correlations. A later study (Xu et al., 1993) was conducted considering a detailed reaction mechanism. The obtained numerical results for a segregated mesh showed smaller deviations from the experimental data obtained by Mitchell et al. (1980) than the numerical predictions of the same authors.

Tarhan and Selçuk (2003) conducted a numerical study using the Method of Lines in a parallelized computational code to solve a reactive flow similar to the one in Mitchell et al. (1980). The flame sheet model was used and the obtained

numerical results were compared with numerical data in the literature (Xu and Smooke, 1993) showing good agreement with both experimental (Mitchell et al., 1980) and numerical data (Xu and Smooke, 1993). Tarhan and Selçuk (2007) in a later study evaluated the influence of detailed reaction mechanisms and thermophysical properties variations for the same flow field configuration. Results for both transient and steady-state flow regime were presented. The steady-state flow results were compared to experimental data (Mitchell et al., 1980) and showed a better agreement than previously obtained in Tarhan and Selçuk, 2003 due to the enhanced descriptions used for the chemical kinetic model and for the thermophysical property variations.

Cunha and Veras (2021) carried out 3D numerical simulations of the burner studied in (Mitchell et al., 1980), using the flame sheet model, replicating the near-wall gas temperature and injection velocity profiles for perforated plate burners with varying number of passages. Notably, the discrete nature of fuel and oxidizer injection at the inflow plane was shown to significantly influence the flame shape and length. The numerical predictions closely matched the experimental data, especially concerning the flame structure, mass fractions, and temperature distribution for non-premixed laminar flames, regardless of the chosen combustion model. The study also revealed that increasing burner porosity leads to a decrease in flame length up to a limiting value.

Soares-Júnior and Leiroz (2022) conducted a numerical study on preferential diffusion effects in a laminar coflowing jet flame using an extended Shvab-Zel'dovich formulation. Results were validated against unity Lewis number case and showed good agreement with experimental (Mitchell et al., 1980) and numerical data (Xu and Smooke 1993; Tarhan and Selçuk 2003; Sauer 2012; Dasgupta, Gonzalez-Juez, and Haworth 2019; Cunha and Veras 2021), regardless the inclusion of thermal radiation effects and detailed kinetic models. Besides, results also showed that the use of a flame sheet model reduced the need for grid refinement near the flame regions, due to the smooth and monotonic solution behavior of mixture fraction and excess enthalpy instead of temperature and mass fractions.

After reviewing the literature, it is possible to note that the heat transfer effects of the solid burner walls has not received much attention for jet diffusion flames. Nevertheless, solid wall thermal influence has been investigated in studies involving porous media (Ferguson et al., 2021; Kokubun et al., 2017) and confined pre-mixed flames (Rahbari et al., 2021) showing the importance of heat diffusion within solids on different the reactive flow phenomena. Furthermore, experimental studies on micro-combustors showed that different flame regimes were observed for similar size burners built of materials with different thermophysical properties (Sirignano et al., 2002). The present study seeks to investigate the thermal phenomena between a surrounding burner solid wall and the diffusion-controlled reactive flow.

2. MATHEMATICAL MODEL

A sketch of the solution domain where the solution is sought is shown in Fig. 1. A concentric cylindrical tube burner, showing the coordinate system used and the main dimensions of the burner is shown. At the burner inlet ($x = 0$), fuel and oxidant streams are admitted through the inner tube ($r < R_F$) and the annular space ($R_F < r < R_O$), respectively, with their respective uniform velocity profile. The burner outlet ($x = L$) is open to the surrounding atmosphere and, therefore, to uniform pressure. The outer wall of the burner ($r = R_O$) can be in a thermally condition of constant temperature in the present work. For the introductory wall temperature effects study discussed in the present work, the improved description of the inlet flow profile (Cunha and Veras 2021) and backward mass diffusions effects (Xu and Smooke, 1993) were neglected.

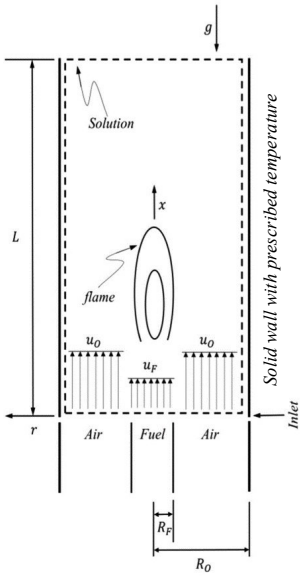

Figure 1. Sketch of the physical domain (Soares-Júnior and Leiroz, 2022).

For the present analysis, the conservation equations are written in transient form assuming Newtonian behavior and that the only body force acting on the flow is gravity. It is considered that the flow occurs at low velocities and that the gases have low absorptivity and, therefore, the effects of thermal radiation, viscous dissipation and pressure work can be neglected. Soret and Dufour effects are also neglected, while heat and mass fluxes obey Fourier's and Fick's laws, respectively. It is also assumed constant specific heats for all species involved in the flow. Besides, the Burke-Schumman limit is considered for the reactive flow.

An extension of the classic Shvab-Zel'dovich formulation (Fachini, 2007; Liñán, 2002) for diffusive flame problems is used in order to consider non-adiabatic boundaries. In addition, the limiting case of the unity Lewis number is considered to isolate the surrounding wall temperature effects in the reactive flow. The governing equations are written in axisymmetric cylindrical coordinates in conservative form in primitive variables as

$$\frac{\partial \rho}{\partial t}+\frac{1}{r}\frac{\partial}{\partial x}(\rho r u)+\frac{1}{r}\frac{\partial}{\partial r}(\rho r v)=0 \tag{1}$$

$$\frac{\partial}{\partial t}(\rho u)+\frac{1}{r}\frac{\partial}{\partial x}(\rho r u u)+\frac{1}{r}\frac{\partial}{\partial r}(\rho r u v)=-\frac{\partial p}{\partial x}+\frac{1}{r}\frac{\partial}{\partial x}\left(r\mu\frac{\partial u}{\partial x}\right)+ +\frac{1}{r}\frac{\partial}{\partial r}\left(r\mu\frac{\partial u}{\partial r}\right)+\frac{1}{r}\frac{\partial}{\partial r}\left(r\mu\frac{\partial v}{\partial x}\right)+\frac{1}{3}\frac{1}{r}\frac{\partial}{\partial x}\left(r\mu\frac{\partial u}{\partial x}\right)-\frac{2}{3}\frac{1}{r}\frac{\partial}{\partial x}\left[\mu\frac{\partial (rv)}{\partial x}\right]-\rho g \tag{2}$$

$$\frac{\partial}{\partial t}(\rho v)+\frac{1}{r}\frac{\partial}{\partial x}(\rho r u v)+\frac{1}{r}\frac{\partial}{\partial r}(\rho r v v)=-\frac{\partial p}{\partial r}+\frac{1}{r}\frac{\partial}{\partial x}\left(r\mu\frac{\partial v}{\partial x}\right)+ +\frac{1}{r}\frac{\partial}{\partial r}\left(r\mu\frac{\partial v}{\partial r}\right)+\frac{1}{r}\frac{\partial}{\partial r}\left(r\mu\frac{\partial v}{\partial r}\right)+\frac{1}{r}\frac{\partial}{\partial x}\left(r\mu\frac{\partial u}{\partial x}\right)-\frac{2}{3}\frac{1}{r}\frac{\partial}{\partial r}\left[\mu\frac{\partial (rv)}{\partial x}\right]+ -\frac{2}{3}\frac{1}{r}\frac{\partial}{\partial r}\left[\mu\frac{\partial u}{\partial x}\right]-\frac{2\mu}{r^2}+\frac{2}{3}\frac{\mu}{r^2}\frac{\partial}{\partial r}(rv)+\frac{2}{3}\frac{\mu}{r}\frac{\partial u}{\partial x} \tag{3}$$

$$\frac{\partial}{\partial t}(\rho Z)+\frac{1}{r}\frac{\partial}{\partial x}(\rho r u Z)+\frac{1}{r}\frac{\partial}{\partial r}(\rho r v Z)=\frac{1}{Le(Z)}\left\{\frac{1}{r}\frac{\partial}{\partial x}\left[\rho r\mathbb{D}\frac{\partial Z}{\partial x}\right]+\frac{1}{r}\frac{\partial}{\partial r}\left[\rho r\mathbb{D}\frac{\partial Z}{\partial r}\right]\right\} \tag{4}$$

$$\frac{\partial}{\partial t}(\rho H)+\frac{1}{r}\frac{\partial}{\partial x}(\rho r u H)+\frac{1}{r}\frac{\partial}{\partial r}(\rho r v H)=\frac{1}{r}\frac{\partial}{\partial x}\left[\rho r\mathbb{D}\frac{\partial H}{\partial x}\right]+\frac{1}{r}\frac{\partial}{\partial r}\left[\rho r\mathbb{D}\frac{\partial H}{\partial r}\right]+ -\frac{N(Z)}{Le(Z)}\left\{\frac{1}{r}\frac{\partial}{\partial x}\left[\rho r\mathbb{D}\frac{\partial Z}{\partial x}\right]+\frac{1}{r}\frac{\partial}{\partial r}\left[\rho r\mathbb{D}\frac{\partial Z}{\partial r}\right]\right\} \tag{5}$$

$$\rho=\frac{p\overline{W}}{R_u T} \tag{6}$$

where x, r, t are the axial and radial coordinates and time, respectively, and u, v, p and T represents the axial and radial velocities, pressure, and temperature, respectively. Besides, density, the dynamic viscosity, the mass diffusion coefficient, the universal ideal gas constant, the molecular weight and the gravity acceleration are represented by ρ, μ, $\mathbb{D}$, R_u, $\overline{W}$ and g, respectively.

The extended Shvab-Zel'dovich formulation allows the elimination of the non-linear reaction source terms on both mass and energy conservation equations by using the mixture fraction (Z) and the excess enthalpy (H) functions, defined as

$$Z=\frac{S\hat{Y}_F-\hat{Y}_O+1}{S+1} \qquad H=\hat{Y}_F+\hat{Y}_O-1+(1+S)Le_F c_p(T-T_{O,i})\frac{1}{qY_{F,i}} \tag{7}$$

where $\hat{Y}_F=Y_F/Y_{F,i}$ and $\hat{Y}_O=Y_O/Y_{O,i}$ are the normalized fuel and oxidant mass fraction, respectively, and $S=s_O Y_{F,i}Le_O/Y_{O,i}Le_F$ is the generalized mass stoichiometric coefficient. Besides, $Y_{F,i}$ and $Y_{O,i}$ represent the fuel and oxidant mass fraction in the inlet section, respectively. The mass stoichiometric coefficient, the fuel and oxidant Lewis number are represented by s_O, Le_F and Le_O.

The parameters $Le(Z)$ and $N(Z)$ are defined as

$$Le(z)=\begin{cases}Le_O, & Z\le Z_f\\ Le_F, & Z>Z_f\end{cases} \qquad N(Z)\begin{cases}(1-Le_O)(S+1), & Z\le Z_f\\ (Le_F-1)(S+1)/S\ , & Z>Z_f\end{cases} \tag{8}$$

where Z_f is the mixture fraction value along the flame location, defined as

$$Z_f = \frac{1}{S+1} = \left(1 + \frac{s_O Y_{F,i}}{Y_{O,i}} \frac{Le_O}{Le_F}\right)^{-1} \tag{9}$$

The system of governing equations (Eqs. 1-6) is subject to boundary conditions written as

$$\frac{\partial u}{\partial r} = v = \frac{\partial P}{\partial r} = \frac{\partial Z}{\partial r} = \frac{\partial H}{\partial r} = 0; \qquad 0 < x < L, \qquad r = 0, \qquad t > 0, \tag{10}$$

$$\frac{\partial u}{\partial x} = \frac{\partial v}{\partial x} = \frac{\partial Z}{\partial x} = \frac{\partial H}{\partial x} = 0, \qquad p = p_a; \qquad x = L, \qquad 0 < r < R_O, \qquad t > 0, \tag{11}$$

$$u = u_{F,i}, \qquad v = 0, \qquad Z = 1, \qquad H = 0; \qquad x = 0, \qquad 0 < r < R_F, \qquad t > 0, \tag{12}$$

$$u = u_{O,i}, \qquad v = 0, \qquad Z = 0, \qquad H = 0; \qquad x = 0, \qquad R_F < r < R_O, \qquad t > 0, \tag{13}$$

$$u = v = \frac{\partial Z}{\partial r} = 0; \qquad 0 < x < L, \qquad r = R_O, \qquad t > 0, \tag{14}$$

The boundary condition for the excess enthalpy (H) (Eq. 5) presents two possible cases for the inner wall of the outer tube ($r = R_O$): Neumann and Dirichlet boundary conditions, defined as

$$\theta_1 (H - H_w) - \theta_2 \frac{\partial H}{\partial r} = 0; \qquad 0 < x < L, \qquad r = R_O, \qquad t > 0, \tag{15}$$

where θ_1 and θ_2 are parameters. Equation 15 is written for an adiabatic wall boundary condition when $\theta_1 = 0$ and $\theta_2 = 1$; and the prescribed temperature boundary condition when $\theta_1 = 1$ and $\theta_2 = 0$. Besides, H_w is defined as

$$H_w(Z_w) = \hat{Y}_{F,w}(Z_w) + \hat{Y}_{O,w}(Z_w) - 1 + (1+S) Le_F c_p (T_w - T_{O,i}) \frac{1}{q Y_{F,i}} \tag{16}$$

where $\hat{Y}_{F,w}(Z_w)$ and $\hat{Y}_{O,w}(Z_w)$ represent the normalized mass fractions of fuel and oxidant in the wall, respectively, and T_w is the prescribed wall temperature value. Particularly, for over-ventilated flames, H_w is a function of the oxidant mass fraction solely. To conduct the pseudo-transient calculations, the initial condition is established as a stagnant isothermal oxidant-filled solution domain. Once the system of governing equations subjected to the boundary conditions (Eqs 10-15) are solved, the primitive variables, Y_F, Y_O and T, are recovered by applying the Eq. 7.

The dependence of the specific mass is considered as of the ideal gas equation of state (Eq. 6), and the dynamic viscosity and the mass diffusion coefficient are defined as

$$\rho \mathbb{D} = \frac{\mu}{Pr_{ref}}, \qquad \mu = \mu_{ref} \left(\frac{T}{T_{ref}}\right)^{\gamma} \tag{17}$$

where, according to the literature (Xu and Smooke, 1993; Tarhan and Selçuk, 2003), $\gamma = 0.7$, $T_{ref} = 298$ K, $\mu_{ref} = 1.85 \cdot 10^{-4}$ g/cm.s and $Pr_{ref} = 0.75$. To estimate the ratio q/c_p in Eq. 7, an experimentally obtained T_f flame temperature of 2050 K for methane-air combustion is considered (Mitchell et al., 1980), thus the expression for H (Eq. 7) is reduced, considering the assumption of unity Lewis number, to

$$\frac{q}{c_p} = \frac{1}{Y_{F,i}} \left[\left(T_f - T_O\right)(1+S) \right] \tag{18}$$

The relaxation of the non-adiabatic boundary condition (Eq. 16) allows the analysis of the thermal interaction between the burner outer wall and the reactive flow. For such analysis, the local Nusselt number (Nu) is expressed as function of the convective heat transfer coefficient (h) as

$$Nu = \frac{h(x) \mathcal{D}}{\lambda} \qquad h(x) = \frac{-\lambda \left. \frac{\partial T(r,x)}{\partial r} \right|_{r=R_O}}{(T_w - T_m)} \tag{19}$$

where $\mathcal{D}$ is the burner diameter, $\lambda = 26.14 \cdot 10^{-3}\,\mathrm{W/m.K}$ is the thermal conductivity and T_m is the mixed mean temperature (Eq. 21)

$$T_m(x) = \frac{\int_0^{Ro} u(r)T(r,x)2\pi r dr}{\int_0^{Ro} u(r)2\pi r dr} \tag{20}$$

3. NUMERICAL APPROACH

The numerical solution of Eqs. 1-6 is based on a computational code developed using the Finite Volume Method (FVM) in the present work. A numerical mesh generation using Poisson's partial difference equation was used to control grid points arrangement in the solution domain. The convective and diffusive terms were evaluated via the Weighted Upstream Differencing Scheme (WUDS) (Raithby and Torrance, 1974) while the Semi-Implicit Method for Pressure Linked Equations-Consistent (SIMPLEC) (Van Doormaal and Raithby, 1984) was used for the pressure-velocity coupling. Besides, the boundary conditions were discretized using fictitious volumes. The linear algebraic system generated by the discretization procedure were solved by using both Successive over-relaxation (SOR) and Alternative Direction Implicit (ADI) methods (Pletcher et al., 1997). Studies of grid convergence, validation and verification of the obtained numerical results were conducted considering the limiting case of unity Lewis number and adiabatic wall boundary condition. Numerical consistency was achieved for a mesh of 320x320 internal points. Moreover, good agreement between numerical data in the literature (Mitchell et al., 1980; Xu and Smooke, 1993; Tarhan and Selçuk, 2003; Sauer, 2012) and the obtained numerical results was obtained. The convergence of the grid generation procedure is considered for variations smaller than 10^{-10}. The solution of the discretized conservation equations using SOR method is converged when corrections smaller than 10^{-7} are reached. Besides, the solution of the pressure system using ADI method is obtained for variations smaller than 10^{-2}. The tolerance for the pressure-velocity coupling and the thermophysical properties updating procedure is 5×10^{-6}. The simulations were performed in a desktop computer with 2 deca-core 2.5 GHz processor and 32 GB DDR3 memory showing a physical time approximately 320 h in each run. For the sake of completeness, a more detailed numerical approach analysis was showed in Soares-Junior and Leiroz (2022).

4. RESULTS

A parametric study was conducted to evaluate T_w effects on both temperature and reactants concentration fields, and on the geometric parameters of a laminar diffusion methane flame. The present study analyzes T_w equals to 373 K, 523 K, 773 K, 1023 K, 1273 K and 1523 K. The present results are also obtained considering the geometric and burner operational conditions described in Tab. 1. The chosen temperature range (T_w) is motivated by heat transfer processes in fire tube boilers in which the steam temperature may reach up to 873 K (600°C). (Kitto and Stultz, 2005).

Table 1. Operational conditions.

Geometric Parameters	$R_O = 2.54$ cm	$R_F = 0.635$ cm	$L = 30$ cm
Operational conditions	Fuel Side @ $0 < r < R_F, x = 0$	Air Side @ $R_F < r < R_O, x = 0$	
Axial input velocity	$u_F = 4.5\ cm/s$	$u_O = 9.88$ cm/s	
Radial input velocity	$v_F = 0$ cm/s	$v_O = 0$ cm/s	
Mass fraction	$Y_{CH_4} = 1.0$	$Y_{O_2} = 0.232, Y_{N_2} = 0.768$	
Input temperature	$T_{in} = 298$ K @ $0 < r < R_O, x = L$		
Output pressure	$p_a = 1.0$ atm @ $0 < r < R_O, x = L$		
Chemical reaction	$CH_4 + 2(O_2 + 3.76N_2) \rightarrow CO_2 + 2H_2O + 7.52N_2$		
Reynolds number	$Re = 2R_O u_O \rho / \mu = 317.6$		
Gravity	g = 9.81 m/s (Axial direction; opposite to the fluid flow)		

The effects of surrounding wall temperature on the CH_4 and of O_2 radial mole fraction profiles are shown in Fig. 2. It is observed that in the axial positions of $x = 1.2$ cm and 2.4 cm (Fig. 2a-b) the temperature T_w has a small influence on the molar fractions profiles. For these positions closer to the burner inlet plane, the oxidant entering at a lower temperature ($T_O = 298\,K$) prevent the thermal boundary layer heated by the wall from influencing the molar concentrations. At $x = 5.0$ cm (Fig. 2c), as the wall temperature decreases the reactant molar fractions profiles shift inwards to the symmetry axis, inducing a slender flame.

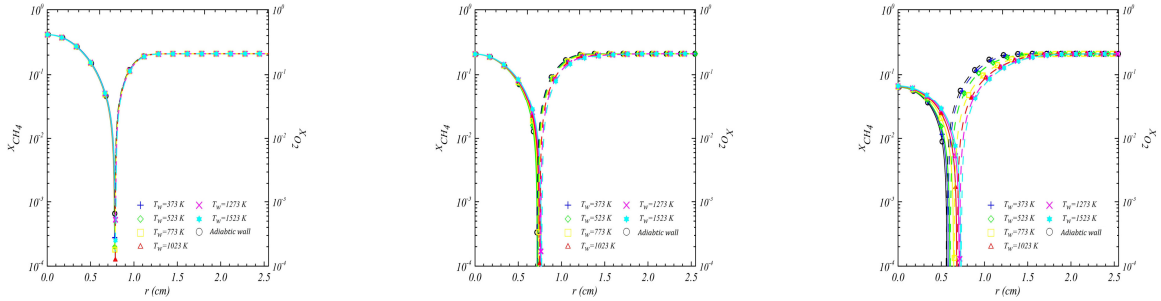

(a) (b) (c)

Figure 2. CH_4 molar fraction (solid lines) and O_2 molar fraction (dashed lines) profiles for different T_w at the axial positions: (a) 1.2 cm; (b) 2.4 cm; (c) 5.0 cm.

Figure. 3a shows the effects of surrounding wall temperature on radial temperature profiles and on temperature distribution along the symmetry axis. A small influence of T_w is noted in the temperature profile along the symmetry axis. In this case, superadiabatic temperatures are observed due to the variation of thermophysical properties, which influence both heat and mass transports to the flame surface. A comparison of the peak temperature between the adiabatic wall case ($T_f = 2050$ K) and the parametric study, shows deviations smaller than 5 %. An increase of the flame height is also observed, considering that the flame axial position is located on the peak temperature.

In the radial temperature profile at the axial position $x = 1.2$ cm (Fig. 3b), it is observed that T_w has no observable influence on the region delimited by the flame surface and the burner symmetry plane. At this position, the oxidant flow is at a lower temperature than the prescribed wall temperature, creating a cold fluid layer that blocks the T_w influence on the flame surface region. Closer to the outer burner wall ($r = R_O$), as T_w increases, the radial temperature profiles become steeper due to the heat flux from the wall to the fluid. In the axial positions of $x = 2.4$ cm and 5.0 cm (Fig. 3c-d), the surrounding wall temperature starts to influence the flame region, leading to the temperature peaks to a radial outward displacement to the symmetry axis as T_w increases. It is also showed that the radial temperature profiles, closer to the flame surface, become steeper as T_w decreases. This effect is caused by the buoyancy increase due to the convective heat transport enhancement in both radial and axial directions. Close to $r = R_O$ it is also observed, as T_w increases the flow becomes more viscous, inducing a reduction in the buoyancy effects.

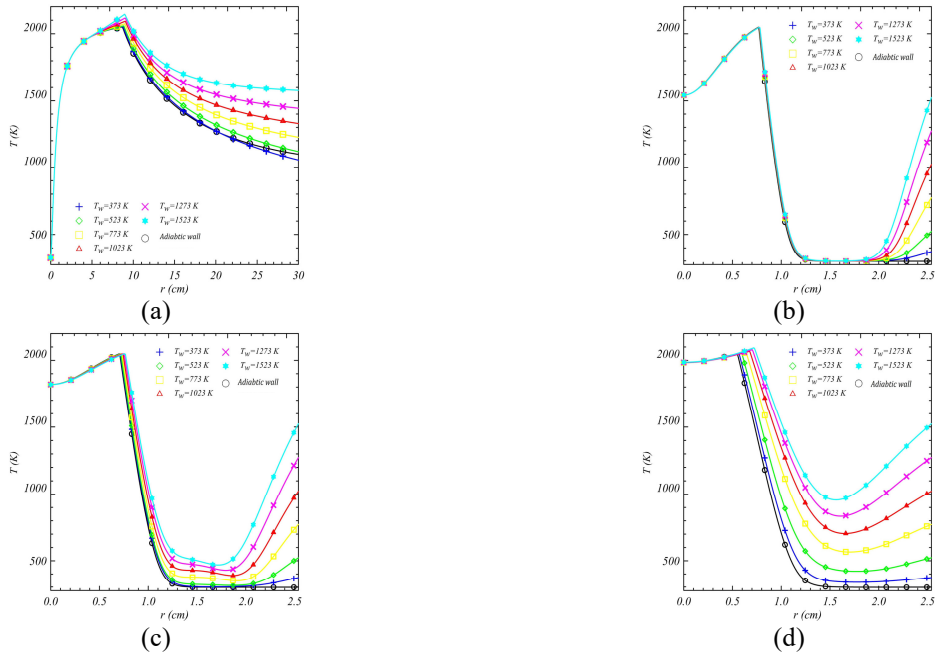

(a) (b) (c) (d)

Figure 3. Temperature profiles for different T_w, (a) along the symmetry axis ($r = 0$) and at the axial positions (b) 1.2 cm; (c) 2.4 cm; (d) 5.0 cm.

Figure 4 shows, respectively, the profiles of the mixed mean temperature (T_m), the temperature difference between the mixed mean temperature and the prescribed wall temperature ($\Delta T = T_m - T_w$), the wall heat flux and the Nusselt

number (Nu) along the outer burner wall ($r = R_O$), considering both reactive and non-reactive situations for comparison purposes. The mixed mean temperature, shown in Fig. 4a, presents a non-monotonic behavior for the reactive problem in contrast to the non-reactive case. In axial positions closer to the flame surface, the heat released by the chemical reaction has a predominant effect, thus disturbing the T_m.behavior. Closer to the outlet burner plane, far from the flame region, a predominant heat loss effect, loads to an asymptotic T_m behavior. It is also possible to notice that this non-monotonic behavior is less pronounced for the cases $T_w = 1273$ K and 1523 K. In these cases, heat loss outside the domain is accentuated, causing the wall to heat the flow.

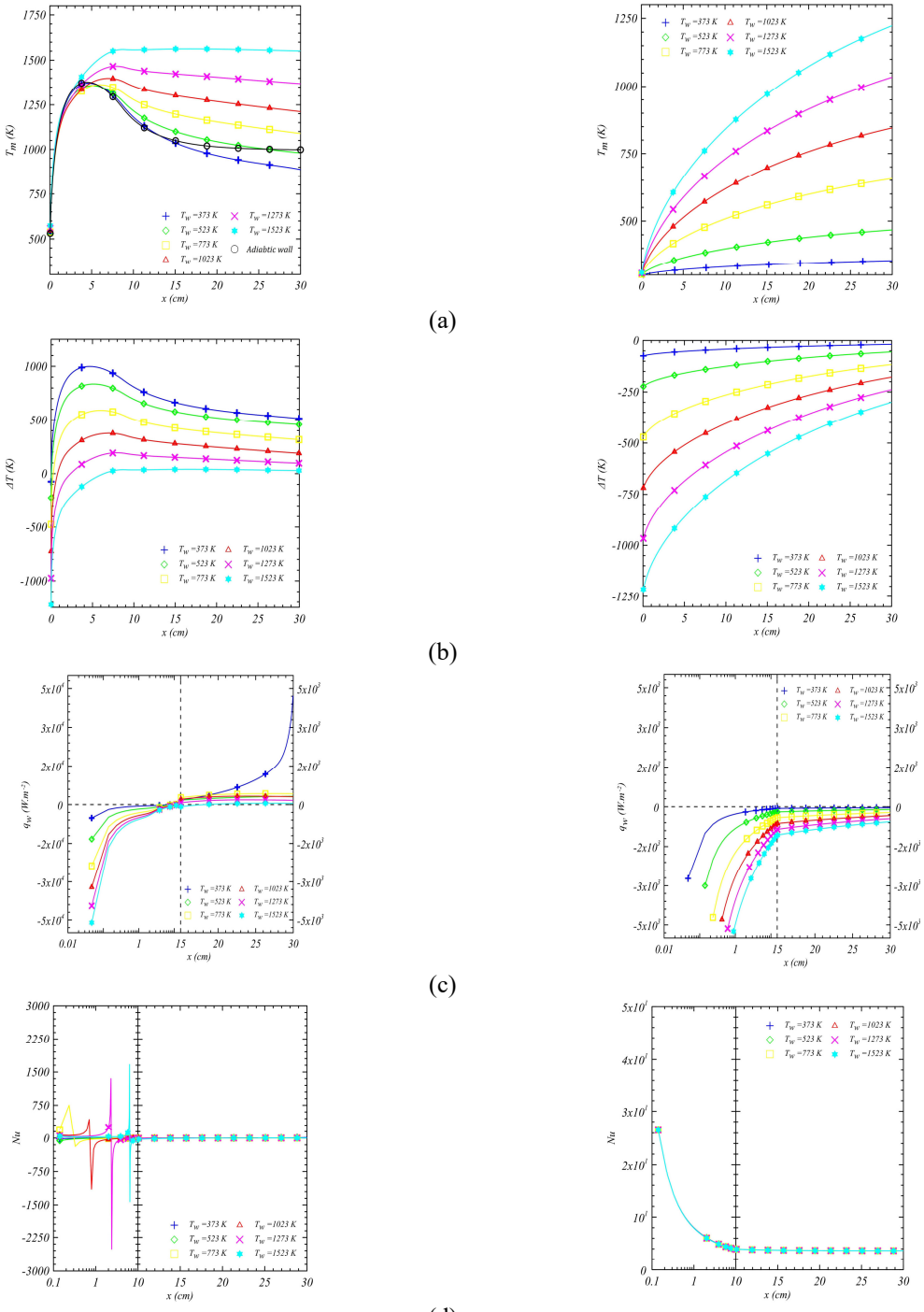

Figure 4. Heat transfer parameters for a reactive flow (left) and for a non-reactive flow (right): (a) mixed mean temperature; (b) $\Delta T = T_m - T_w$; (c) heat flux along the wall; (d) Nusselt number.

Figure 4b shows the difference between the mixed mean temperature and the prescribed wall temperature (ΔT), for the different values of T_w considered. A non-monotonic ΔT behavior, similar to T_m (Fig. 4a) is observed. Negative values

for ΔT are present in the region closer to the burner inlet plane because the reactants entering the burner are colder than the wall. Similarly, to the carried out for the T_m behavior analysis, closer to the flame surface the heat release from the chemical reaction has a predominant effect while far from the flame region, the flow heat loss leads to an asymptotic ΔT behavior in contrast to the non-reactive problem. For the cases $T_w = 1273$ K and 1523 K, it is possible to notice that ΔT has a similar behavior with the non-reactive problem for the corresponding cases.

The heat flux (q_w) along the outer burner wall ($r = R_O$) for the different T_w values, is present in Fig. 4c. It is possible to notice that for all T_w, values, the outer burner wall is heating the flow in the region close to the injection plane ($x = 0$). In this region, the greater the temperature difference between the wall and the incoming fluid, the greater the q_w intensity. For all T_w values considered, the neighboring region of $x = 10$ cm has an inflection point on q_w profiles, contrasting to the non-reactive problem. The inflection point indicates a change in the direction of the heat flux. Therefore, from a certain axial position, the outer burner wall begins to cool the adjacent fluid layer.

Figure 4d shows the effects of surrounding wall temperature on the Nusselt number (Nu) profiles along the outer burner wall. Discontinuities in the Nu number profiles are observed for the cases $T_w = 773$ K, 1023 K, 1273 K and 1523 K, in contrast to the non-reactive case, in which the Nu profiles collapse into a single curve. These discontinuities occurs because ΔT vanishes in a region near $x = 10$ cm, and the heat flux profile changes direction in the wall. It is also possible to observe that in the entrance region the convective heat transport is predominant because of thermal expansion effects, while for positions greater than $x = 10$ cm, diffusive heat transport becomes more predominant. For the T_w values considered, the Nu number profiles have an asymptotic behavior for $x > 10$ cm, which in the limit tends to Nu=3.65 (Cotta and Özışık, 1986), similarly to the non-reactive problem. For the cases of $T_w = 373$ K and 523 K it is not possible to observe the discontinuities in the Nu number profiles, since ΔT (Figs. 4b) becomes null closer to the inlet burner plane and due to the lack mesh refinement in this region.

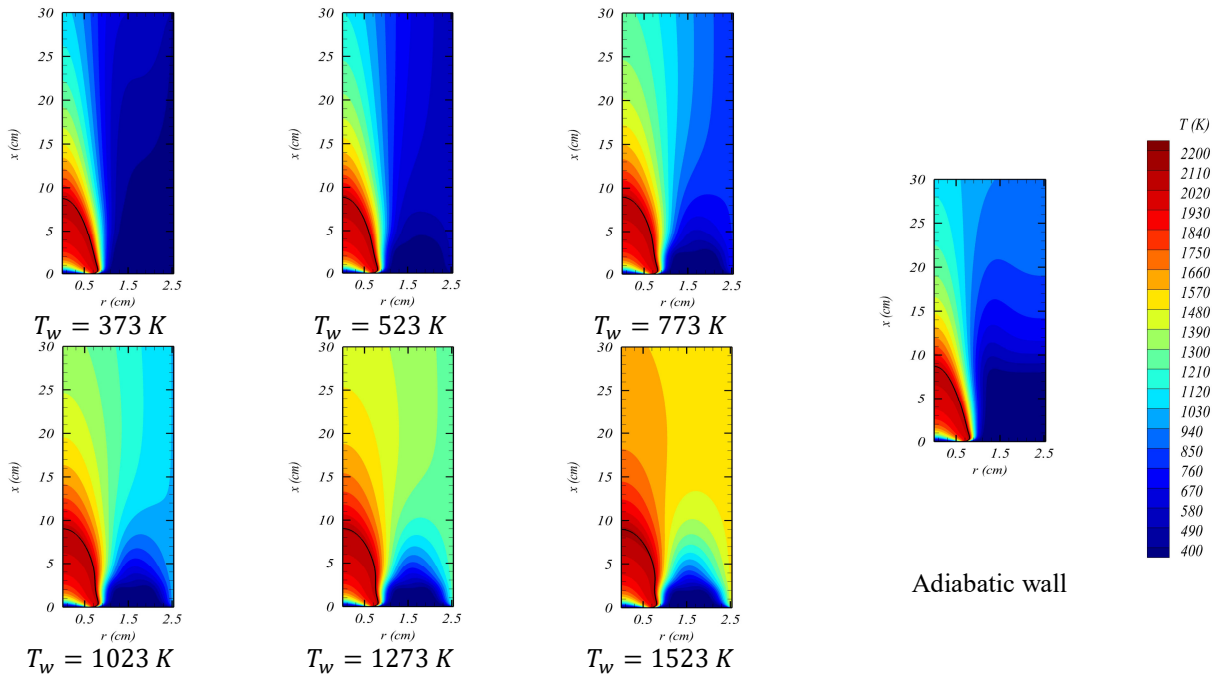

Figure 5. Temperature field and flame shape for a methane flame for the adiabatic wall burner and the burner with surrounding wall temperature.

To complement the previously discussion on the flame displacement, the flame shape and the isotherms within the solution domain are shown in Fig. 5. Decreasing T_w, the flame becomes more slender, due to the temperature field directly influences the thermophysical properties causing this effect. This occurs because the diffusive mass transport is affected by the temperature field. It is also possible to observe the formation of a cold oxidant region closer to the inlet burner plane, between the flame surface and the outer burner wall, due to the oxidant injection at a lower temperature. This region limits the T_w influence on the flame. Longer flames are also observed when T_w increases. In this case, the improvement in the convective heat transport in the axial direction causes an increase in the buoyancy effects conducting a flame elongation. An increase of 4.5% in flame height from the adiabatic wall case is observed. Besides an increase of 22.5%. in flame width at half-height ($x = 4.0$ cm) is also observed in comparison to the adiabatic wall case.Velocity vectors, velocity magnitude, and selected streamlines are shown in Fig. 7. The development of a boundary layer along the outer burner wall and of a shear layer between the fuel and oxidant stream are observed. It is also possible to notice the appearance of recirculation zones for $T_w = 373$ K, 523 K, 773 K, due to the of thermal expansion effects that lead to

an increase in the velocity magnitude near the flame surface. It is observed that for lower T_w values an increase in the recirculation zones conduct to an increase in the velocity magnitude at burner outlet plane. This occurs because the narrowing passage for the flow. It is worth mentioning that a validation study for three tube lengths (30 cm, 60 cm and 90 cm) was also conducted and showed that the recirculation zones near the burner outlet plane does not vary its structure (Soares-Júnior, 2022; Sauer, 2012). For these cases, a cold air flux entering the burner from the recirculation zones close to the outlet plane ($x = L$) is observed. The cold air layer from these zones directly influences the profiles of T_m, ΔT and Nu (Fig. 4). For the cases $T_w = 1023$ K, 1273 K, 1523 K, the absence of recirculation zones indicates that the thermal expansion effects near the flame surface have little effects on the flow. In these cases, as the gas viscosity increases smaller velocity magnitudes are observed.

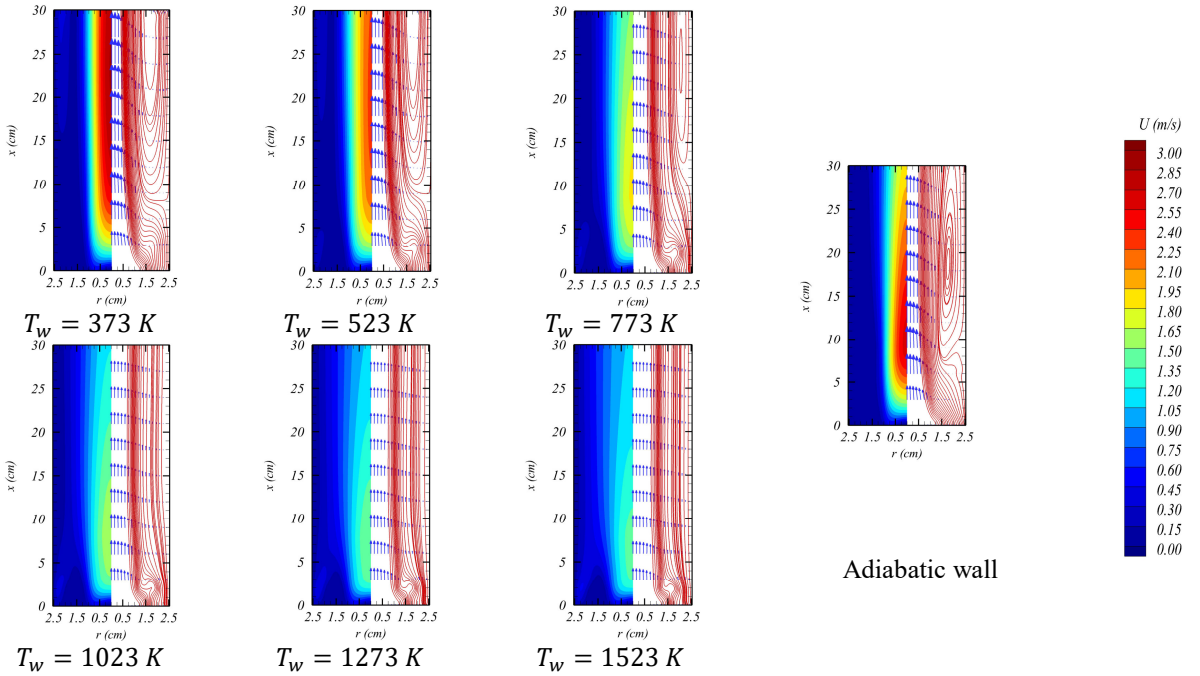

Figure 7. Velocity magnitude, velocity vector and stream function for a methane flame for the adiabatic wall burner and the burner with surrounding wall temperature

5. CONCLUSIONS

This study investigated the impact of surrounding wall temperature (T_w) on laminar diffusion methane flames, covering a range from 373 K to 1523 K. Slender flames were observed for lower T_w values along with reactant profiles shifted away from the burner inlet. Temperature profiles along the symmetry axis exhibited superadiabatic temperatures due to thermophysical property variations, and peak temperature and flame height increased with lower T_w.

The present study also examined mixed mean temperature behavior, temperature differences, wall heat flux, and Nusselt number along the outer burner wall. Reactive conditions led to non-monotonic mean temperature axial profiles, and Nu profiles exhibited discontinuities for certain T_w values. Slender flames and cold oxidant regions near the inlet burner plane were observed with lower T_w. Velocity vectors showed recirculation zones for lower T_w values but not for higher T_w, indicating limited thermal expansion effects.

6. REFERENCES

Burke, S. P., and Schumann, T. E. W. 1928. “Diffusion Flames”. *Industrial & Engineering Chemistry* 20 (10): 998–1004.

Chung, S. H. and Law, C. K. 1984. “Burke–Schumann Flame with Streamwise and Preferential Diffusion”. *Combustion Science and Technology* 37 (1–2): 21–46.

Cotta, R. M. and Özışık, .M. N. 1986. “Laminar Forced Convection of Power-Law Non-Newtonian Fluids Inside Ducts”. *Wärme- Und Stoffübertragung* 20 (3): 211–18.

Cunha, F. A. and Veras, C. A. G. 2021. “Modelling Laminar Diffusion Flames Using a Fast Convergence Three-Dimensional CVFEM Code”. *Combustion Theory and Modelling* 25 (3): 460–87.

Dasgupta, A., Gonzalez-Juez, E. and Haworth, D. C. 2019. “Flame Simulations with an Open-Source Code”. *Computer Physics Communications* 237: 219–29.

Endo Kokubun, M. A., Fachini F. F. and Matalon, M. 2017. "Stabilization and Extinction of Diffusion Flames in an Inert Porous Medium". *Proceedings of the Combustion Institute* 36 (1): 1485–93.

Fachini, F. F. 2007. "Extended Shvab–Zel'dovich Formulation for Multicomponent-Fuel Diffusion Flames". *International Journal of Heat and Mass Transfer* 50 (5–6): 1035–48.

Ferguson, J. C., Sobhani, S., and Ihme, M. 2021. "Pore-Resolved Simulations of Porous Media Combustion with Conjugate Heat Transfer". *Proceedings of the Combustion Institute* 38 (2): 2127–34.

Kitto, J. B., and Stultz, S. C. 2005. *Steam: Its Generation and Use*. 41º ed. Barberton, Ohio, USA: Babcock & Wilcox.

Kuo, K. K. 2005. *Principles of Combustion*. 2nd ed. Hoboken, NJ: John Wiley.

Liñán, A. 2002. "Diffusion-controlled combustion". Em *New Trends in Continuum Mechanics*. New York: E.T.S.I. Aeronáuticos (UPM).

Mitchell, R.E., Sarofim, A. F., and Clomburg, L. A. 1980. "Experimental and Numerical Investigation of Confined Laminar Diffusion Flames". *Combustion and Flame* 37: 227–44.

Patankar, S. V. 1980. *Numerical Heat Transfer and Fluid Flow*. Series in computational methods in mechanics and thermal sciences. Washington : New York: Hemisphere Pub. Corp. ; McGraw-Hill.

Pletcher, R. H., Tannehill, J. C., and Anderson, D A. 1997. *Computational Fluid Mechanics and Heat Transfer*. 2nd ed. Series in computational and physical processes in mechanics and thermal sciences. Washington, DC: Taylor & Francis.

Rahbari, A., Homayoonfar, S., Valizadeh, E., Aligoodarz, M. R., and Toghraie, D. 2021. "Effects of Micro-Combustor Geometry and Size on the Heat Transfer and Combustion Characteristics of Premixed Hydrogen/Air Flames". *Energy* 215: 119061.

Raithby, G.D., and Torrance, K.E. 1974. "Upstream-Weighted Differencing Schemes and Their Application to Elliptic Problems Involving Fluid Flow". *Computers & Fluids* 2 (2): 191–206.

Sauer, V. M. 2012. "Análise de Escoamentos Reativos de Biocombustíveis em Dutos". M.Sc. Dissertation, Rio de Janeiro, RJ, Brasil: Universidade Federal do Rio de Janeiro.

Sirignano, W. A., Pham, T. K., and Dunn-Rankin, D. 2002. "Miniature-Scale Liquid-Fuel-Film Combustor". *Proceedings of the Combustion Institute* 29 (1): 925–31.

Smooke, M. D. 2013. "The Computation of Laminar Flames". *Proceedings of the Combustion Institute* 34 (1): 65–98.

Soares-Júnior, R. L. 2022. "Estudo Computacional de Jatos Reativos Laminares: Efeitos de Difusão Preferencial e de Entrada TermoHidrodinâmica". D.Sc. Tesis, Rio de Janeiro, RJ, Brasil: Universidade Federal do Rio de Janeiro.

Soares-Júnior, R. L., and Leiroz, A. J. K. 2022. "A Numerical Study on Preferential Diffusion Effects in Coflowing Laminar Reacting Jets". *Journal of the Brazilian Society of Mechanical Sciences and Engineering* 44 (1): 12.

Tarhan, T., and Selçuk, N. 2003. "Numerical Simulation of a Confined Methane/Air Laminar Diffusion Flame by the Method of Lines". *Turkish Journal of Engineering and Environmental Sciences* 27 (4).

Tarhan, T., and Selçuk, N. 2007. "A Novel CFD Code Based on Method of Lines for Reacting Flows: Verification on Methane/Air Diffusion Flame". *Combustion Science and Technology* 179 (1–2): 39–60.

Van Doormaal, J. P., and Raithby, G. D. 1984. "Enhancements Of The Simple Method For Predicting Incompressible Fluid Flows". *Numerical Heat Transfer* 7 (2): 147–63.

Williams, F. A. 1985. *Combustion Theory: The Fundamental Theory of Chemically Reacting Flow Systems*. 2nd ed. Combustion science and engineering series. Menlo Park, Calif: Benjamin/Cummings Pub. Co.

Xu, Y., and Smooke, M. D. 1993. "Application of a Primitive Variable Newton's Method for the Calculation of an Axisymmetric Laminar Diffusion Flame". *Journal of Computational Physics* 104 (1): 99–109.

Xu, Y., Smooke, M., Lin, P. and Long, M. B. 1993. "Primitive Variable Modeling of Multidimensional Laminar Flames". *Combustion Science and Technology* 90 (5–6): 289–313.

Zadsirjan, S., Tabejamaat, S., Abtahizadeh, E. and van Oijen, J. 2020. "Large Eddy Simulation of Turbulent Diffusion Jet Flames Based on Novel Modifications of Flamelet Generated Manifolds". *Combustion and Flame* 216: 398–411.

7. RESPONSIBILITY NOTICE

The authors are the only responsible for the printed material included in this paper.